Supporting Information

Syntheses and photocatalytic properties of three new d^{10}-based coordination polymers: Effect of metal centre and ancillary ligands

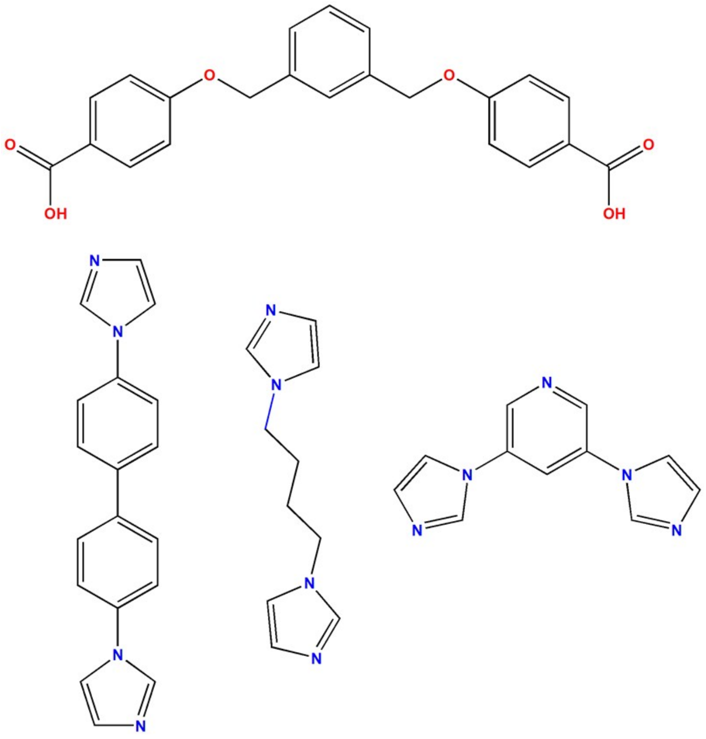

Scheme S1 View of the structure skeletons of the ligands in this work.

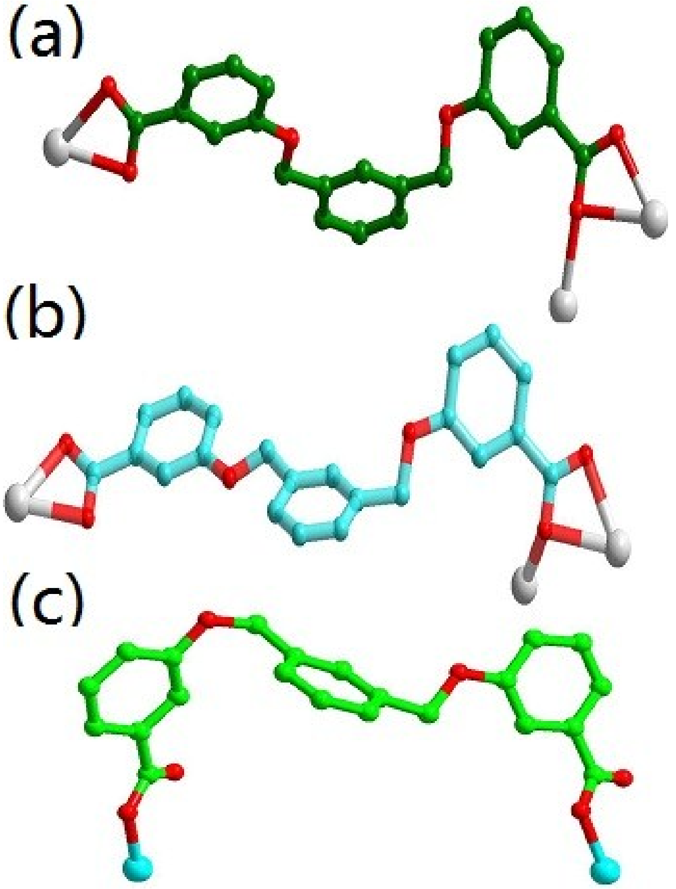

Scheme S2 view of the different coordination modes of H_2Lin **1-3**.

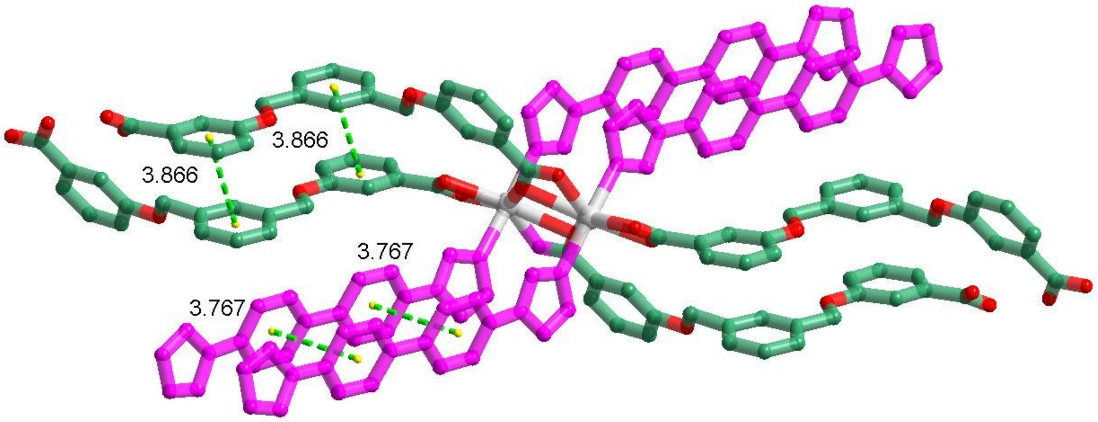

Fig. S1 view of the π–π interactions between the ligands in **1**.

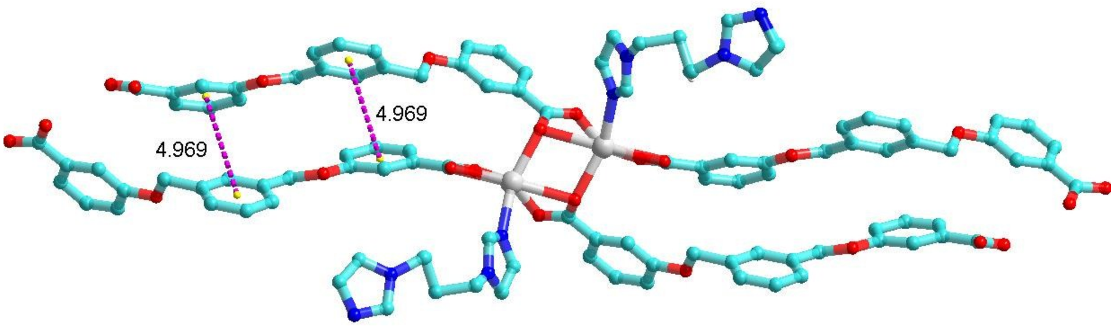

Fig. S2 view of the weak π–π interactions between the ligands in **2**.

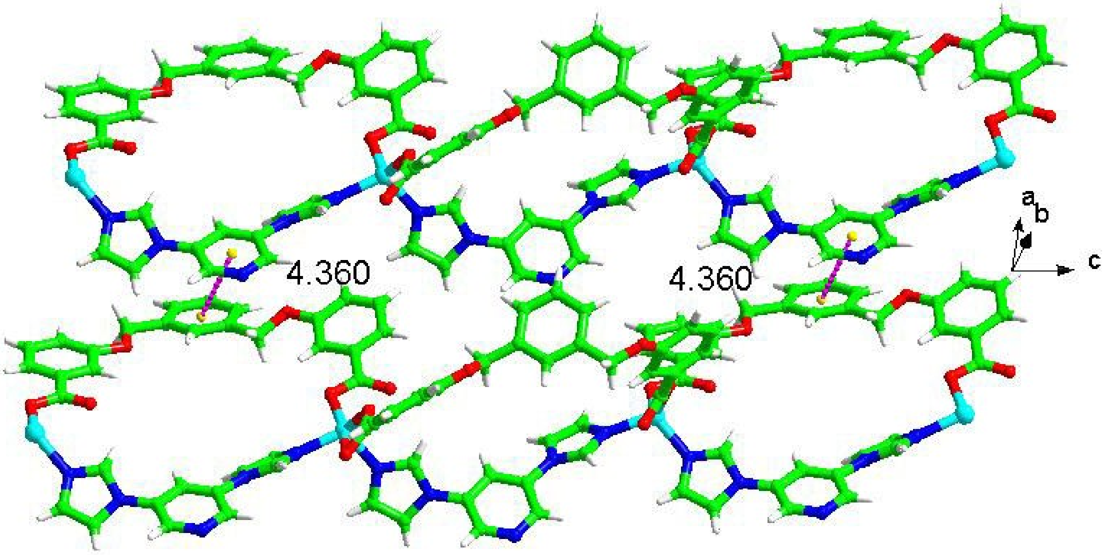

Fig. S3 view of the weak π–π interactions between the ligands from adjacent chains in **3**.

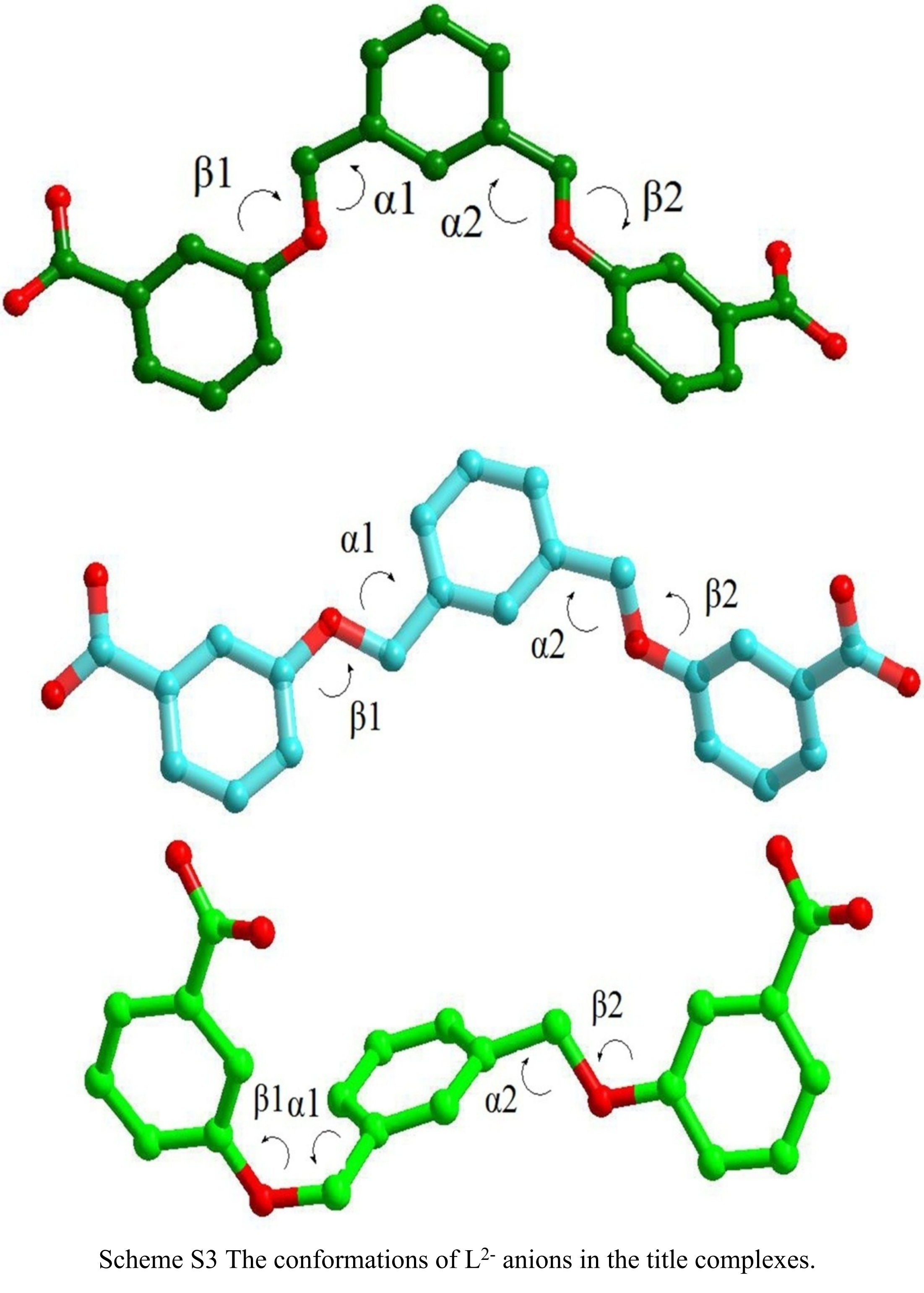

Scheme S3 The conformations of L^{2-} anions in the title complexes.

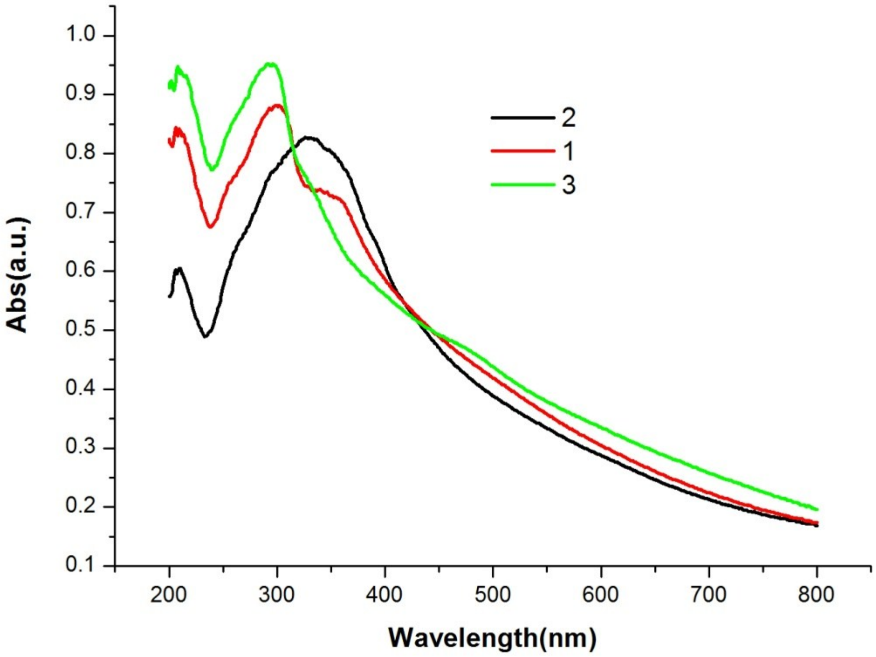

Fig. S4 UV–vis diffuse-reflectance spectra of compounds **1–3** with $BaSO_4$ as background.

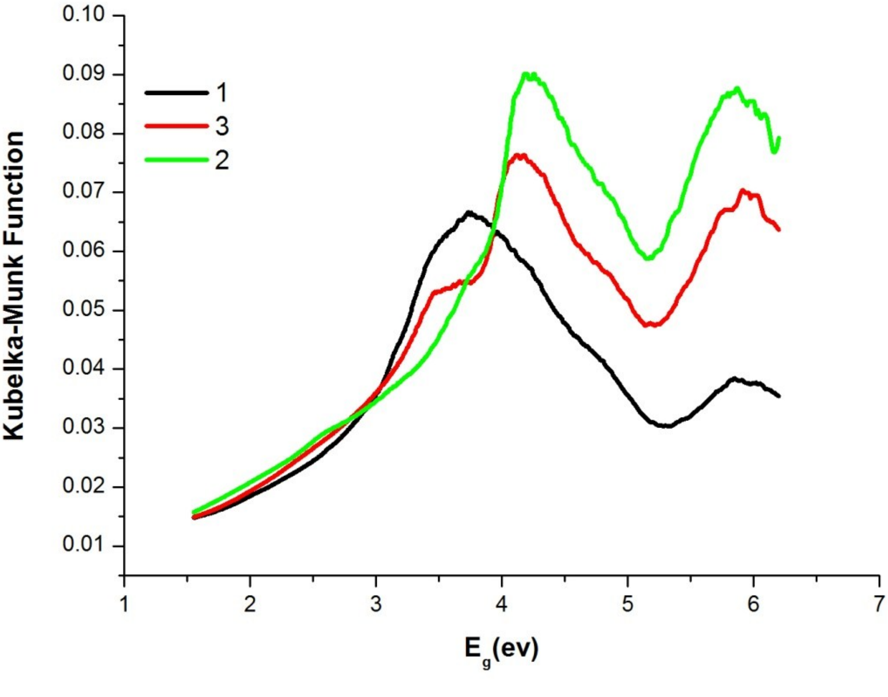

Fig. S5 Solid-state optical diffuse-reflection spectra of **1–3** derived from diffuse reflectance data at ambient temperature.

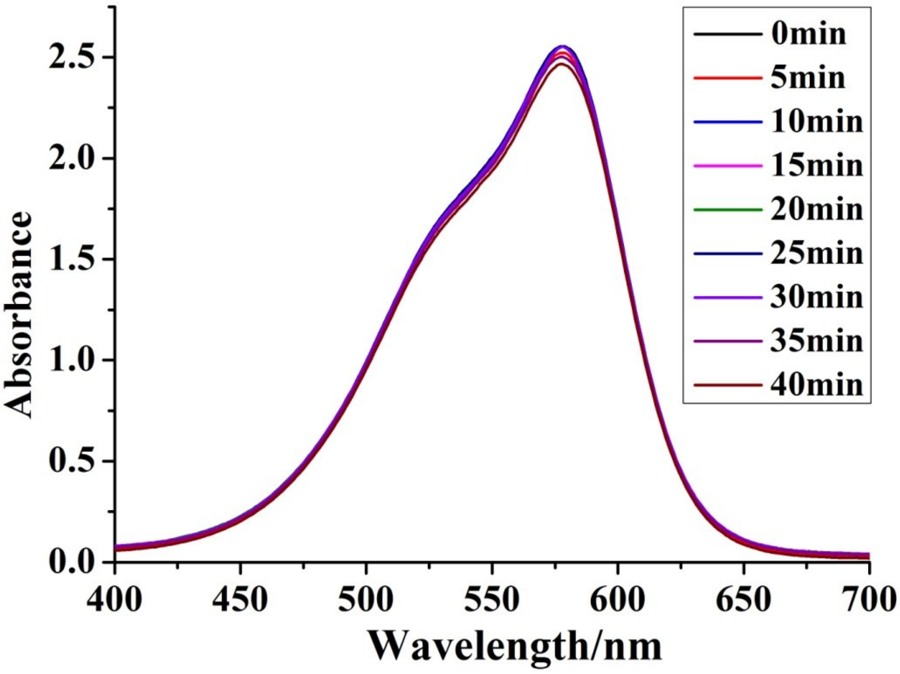

Fig. S6 absorption spectra of the MV solutions during the decomposition reaction under dark condition with the presence of **2.**

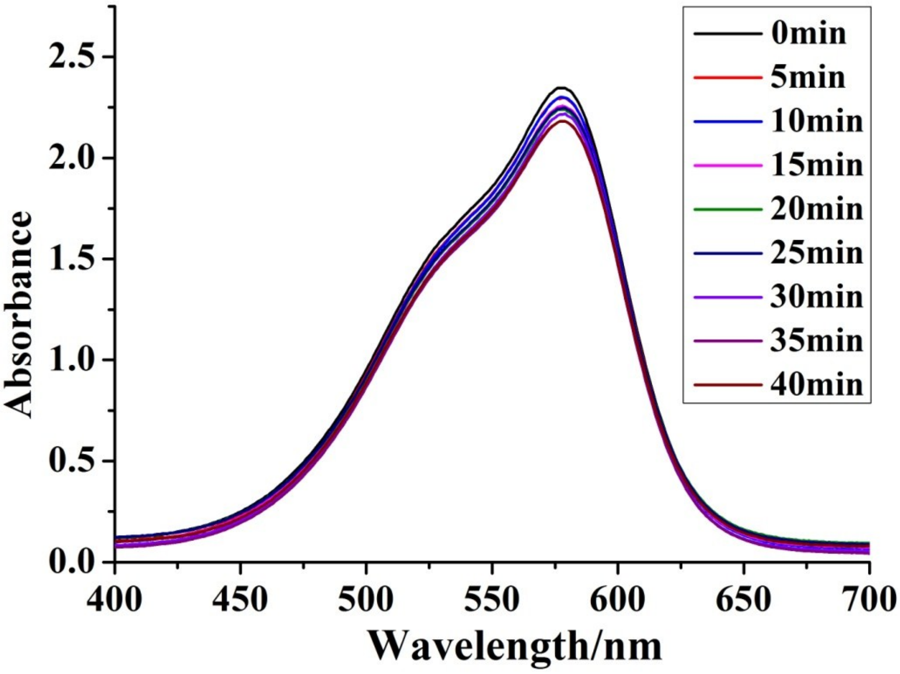

Fig. S7 absorption spectra of the MV solutions during the decomposition reaction under sunlight with the presence of **2.**

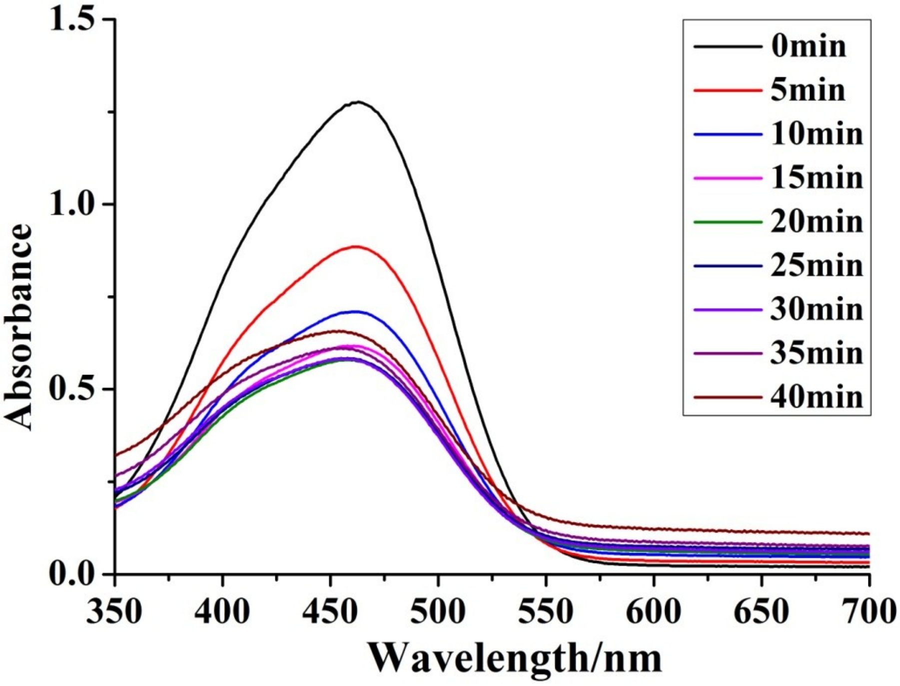

Fig. S8 absorption spectra of the MO solutions during the decomposition reaction under UV-vis with the presence of **2.**

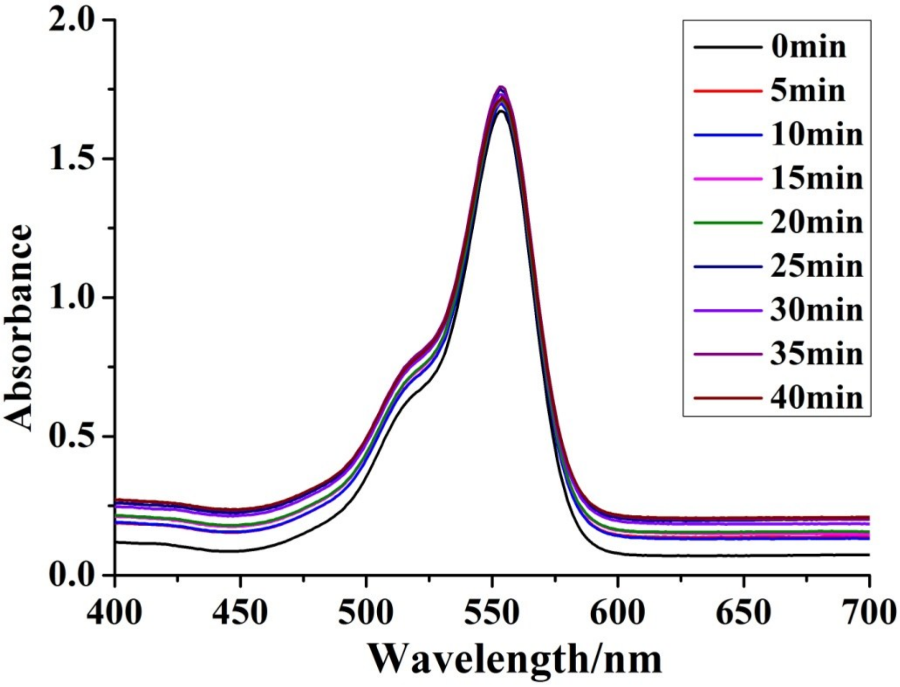

Fig. S9 absorption spectra of the Rh B solutions during the decomposition reaction under UV-vis with the presence of **2.**

IR

The IR spectra of complexes **1–3** are shown in Figs. S10. The strong peaks at *ca*. 1641 and 1209 cm^{-1} may be attributed to the asymmetric and symmetric vibrations of carboxyl groups. The presence of the characteristic bands at 1540, 1564, 1517 and 1386 cm^{-1} suggest the ν(C–N) stretching vibrations of the imidazole ring. In complexes **2**, the IR spectra show the strong absorption bands at 3378 cm^{-1}, which can be considered as m(O–H) of water molecules.

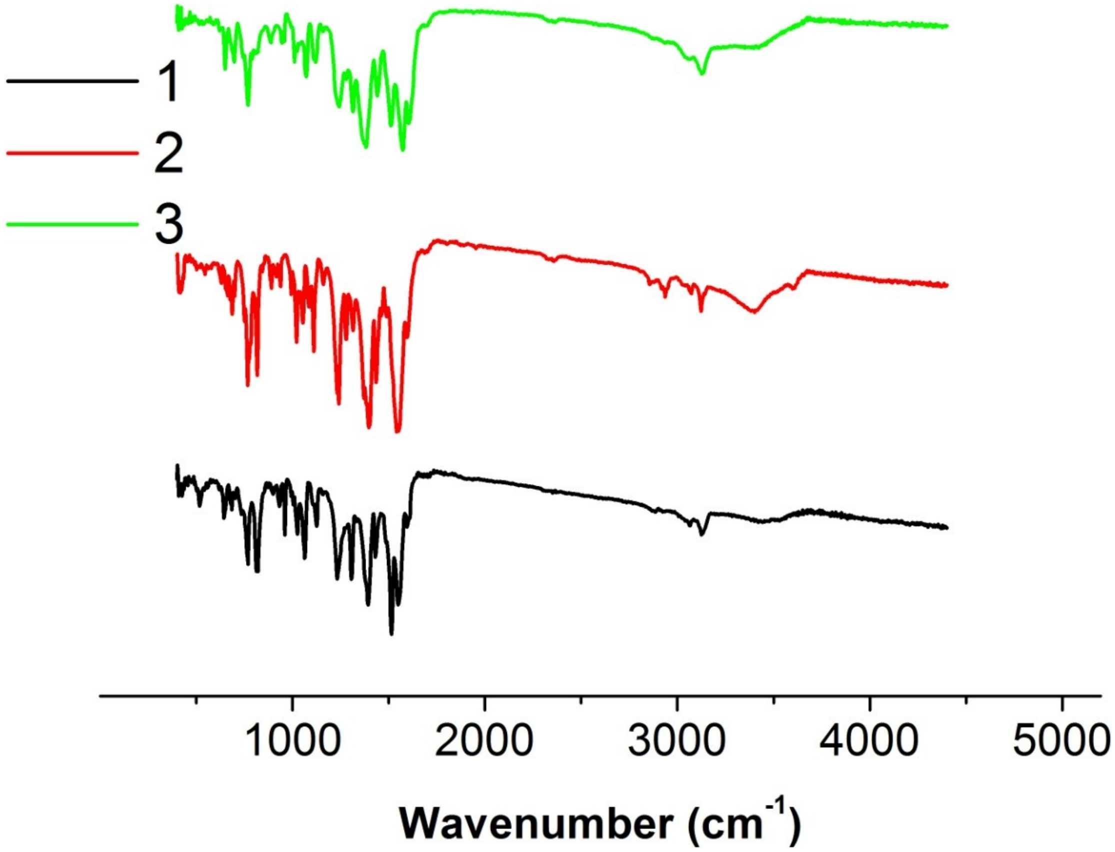

Fig. S10 view of the IR in **1-3**.

Powder X-ray diffraction and thermal stability analyses of complexes **1-3**

The PXRD patterns indicate that the synthesized complexes match with the simulated ones except for some intensity differences, which can be due to the different orientation of the crystals in the powder samples (Fig. S11), proving the crystalline phase purity.

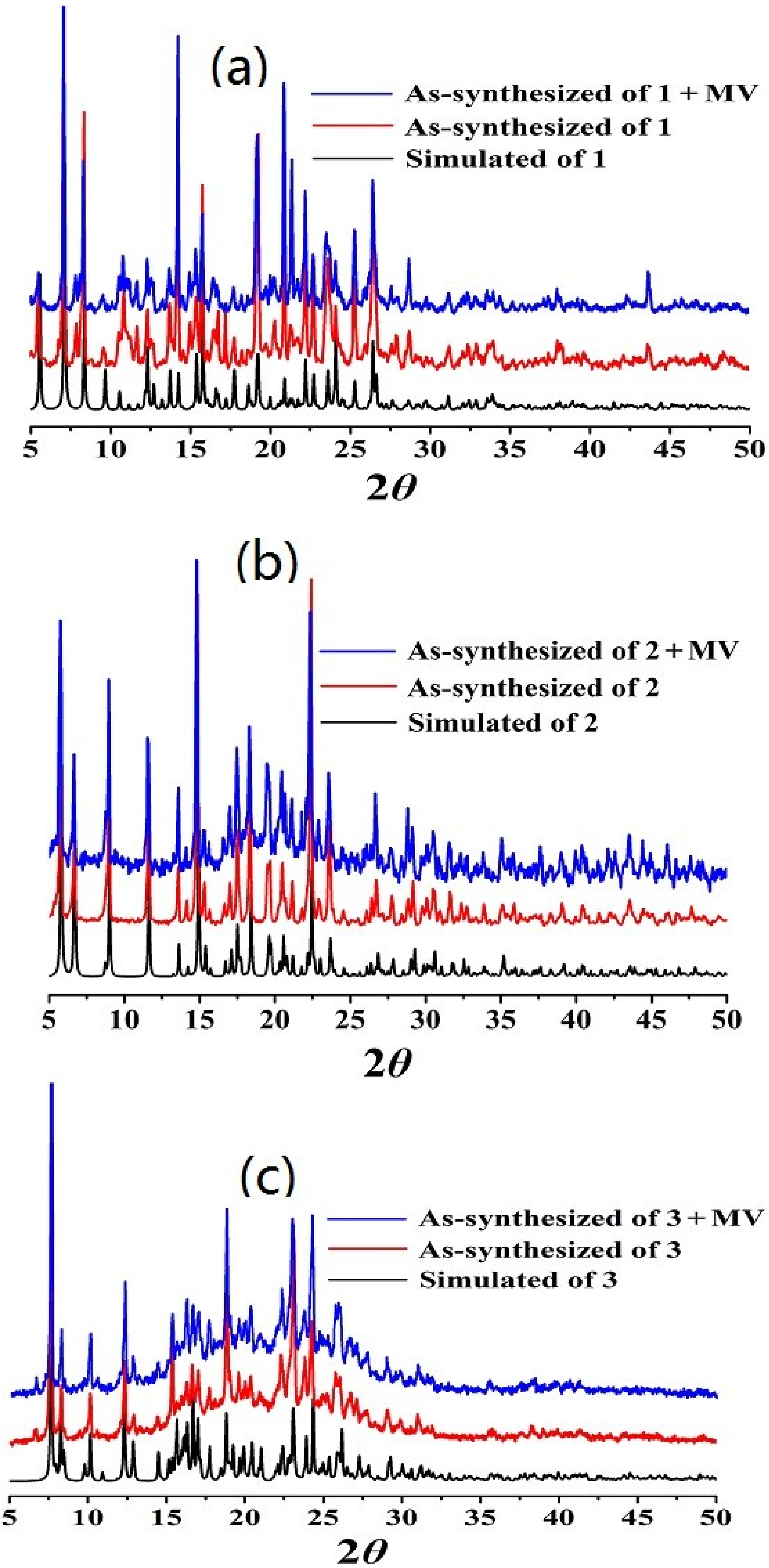

Fig. S11 view of the PXRD patterns of **1** for (a); **2** for (b) and **3** for (c) under the different conditions.

The thermal stabilities of complexes **1-3** are investigated in the temperature range of 20–800 ºC under N_2 atmosphere, as shown in Fig. S12. Complex 2 shows two step of weight losses, respectively. The first weight losses of 2.91% before 255 ºC are consistent with the removal of lattice/coordinated water molecule (calcd. 2.99%). The second weight losses corresponding to the release of organic ligands start at 300 ºC. The remaining residues are assigned to the corresponding metal oxides. The TGA curves for **1** and **3** suggest that their host networks are stable up to 310 and 260 ºC, respectively, then they start to gradually lose their ligands as a result of thermal decomposition.

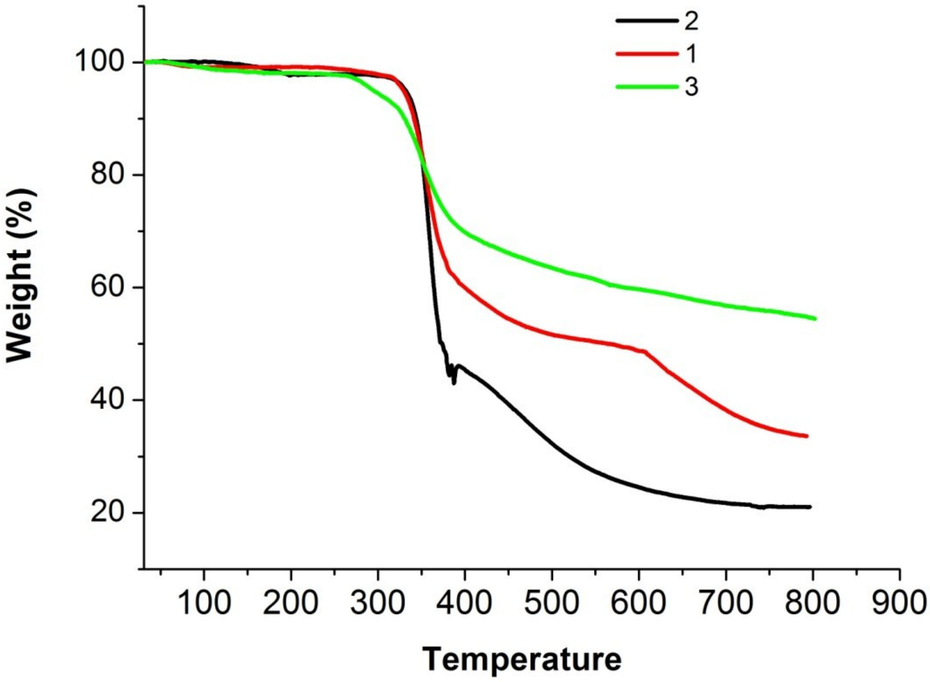

Fig. S12 view of the TGA in this work.

Table S1. Crystallographic data and structure refinement details for Complexes 1-3

Parameter	**1**	**2**	**3**
Formula weight	775.09	601.89	1305.90
Crystal system	Triclinic	Monoclinic	Triclinic
Space group	*P-1*	*P2/n*	*P-1*
Crystal Color	Colorless	Colorless	Colorless
a, Å	8.4912(11)	19.8075(6)	11.1521(4)

b, Å	12.7255(16)	6.2207(2)	12.0285(5)
c, Å	16.048(2)	20.4492(6)	23.5503(7)
α, °	98.133(1)	90	77.262(3)
β, °	91.069(1)	98.035(3)	76.994(3)
γ, °	99.479(1)	90	76.727(3)
V, Å^3	1691.6(4)	2494.94(13)	2947.99(19)
Z	2	4	2
ρ_{calcd}, g/cm^3	1.522	1.602	1.471
μ, mm^{-1}	0.701	7.442	1.623
F(000)	788	1220	1344
θ Range, deg	1.3-27.6	4.4-66.6	3.9-66.6
Reflection Collected	13623	7920	17237
Independent reflections (R_{int})	0.021	0.024	0.022
Reflections with $I > 2\sigma(I)$	6322	3922	8940
Number of parameters	460	391	811
R_1, wR_2 ($I > 2\sigma(I)$)*	0.0322, 0.0903	0.0290, 0.0735	0.0332, 0.0872
R_1, wR_2 (all data)**	0.0422, 0.1068	0.0337, 0.0772	0.0395, 0.0928

* $R = \sum(F_o - F_c)/\sum(F_o)$, ** $wR_2 = \{\sum[w(F_o^2 - F_c^2)^2]/\sum(F_o^2)^2\}^{1/2}$.

Table S2. Selected bond distances (Å) and angles (deg) for **1-3**

		1	
Cd(1)-O(1)	2.493(3)	Cd(1)-O(2)	2.380(2)
Cd(1)-N(1)	2.275(2)	Cd(1)-N(4)#1	2.328(3)
Cd(1)-O(3)#2	2.626(2)	Cd(1)-O(4)#2	2.304(2)
Cd(1)-O(3)#3	2.371(3)		
		2	
Cd(1)-O(1)	2.302(2)	Cd(1)-O(1W)	2.341(3)
Cd(1)-N(1)	2.259(8)	Cd(1)-O(5)#1	2.398(2)
Cd(1)-O(6)#1	2.397(2)	Cd(1)-O(1)#2	2.499(2)
Cd(1)-O(2)#2	2.390(3)	Cd(1)-N(4)#3	2.311(8)
		3	
Zn(1)-O(1)	2.7297(15)	Zn(1)-O(2)	1.9765(15)
Zn(1)-O(7)	1.9541(16)	Zn(1)-N(5)	2.0273(17)
Zn(1)-N(6)	2.0377(17)	Zn(2)-O(12)	1.9351(16)

Zn(2)-N(10)	2.0284(17)	Zn(2)-O(6)#1	1.9571(17)
Zn(2)-N(1)#1	2.0200(17)		

		1	
O(1)-Cd(1)-O(2)	53.81(8)	O(1)-Cd(1)-N(1)	163.30(10)
O(1)-Cd(1)-N(4)#1	98.72(8)	O(1)-Cd(1)-O(3)#2	138.37(8)
O(2)-Cd(1)-N(1)	97.91(8)	O(2)-Cd(1)-N(4)#1	80.78(9)
O(2)-Cd(1)-O(4)#2	136.08(8)	O(2)-Cd(1)-O(3)#3	91.10(8)
N(1)-Cd(1)-N(4)#1	170.21(9)	O(4)#2-Cd(1)-N(1)	101.48(9)
O(3)#2-Cd(1)-N(4)#1	90.57(8)	O(3)#3-Cd(1)-O(4)#2	128.85(8)
		2	
O(1)-Cd(1)-O(1W)	74.76(9)	O(1)-Cd(1)-N(1)	160.6(2)
O(1)-Cd(1)-O(5)#1	93.62(8)	O(1)-Cd(1)-O(6)#1	104.90(8)
O(1W)-Cd(1)-N(1)	89.7(2)	O(1W)-Cd(1)-O(2)#2	143.12(9)
O(5)#1-Cd(1)-N(1)	105.7(2)	O(6)#1-Cd(1)-N(1)	86.1(2)
O(1)#2-Cd(1)-O(5)#1	125.32(7)	O(6)#1-Cd(1)-N(4)#3	90.76(16)
		3	
O(1)-Zn(1)-O(2)	53.37(5)	O(1)-Zn(1)-O(7)	83.68(5)
O(1)-Zn(1)-N(5)	145.73(6)	O(1)-Zn(1)-N(6)	79.72(6)
O(2)-Zn(1)-O(7)	111.72(7)	O(2)-Zn(1)-N(5)	94.84(7)
O(2)-Zn(1)-N(6)	113.16(7)	O(7)-Zn(1)-N(5)	124.58(7)
O(7)-Zn(1)-N(6)	106.03(7)	N(5)-Zn(1)-N(6)	106.38(7)
O(12)-Zn(2)-N(10)	119.59(7)	O(6)#1-Zn(2)-O(12)	110.66(7)
O(12)-Zn(2)-N(1)#1	103.80(7)	N(1)#1-Zn(2)-N(10)	110.60(7)

Symmetry Codes: **For 1**: #1= -1+x, y, -1+z; #2= x, 1+y, 1+z; #3= -x, -y, -z. **For 2**: #1= 3/2-x, y, 1/2-z; #2= 3/2-x, y, 3/2-z; #3= 1-x, 2-y, 1-z. **For 3**: #1= x, y, -1+z.